European Society of Computational Methods in Sciences and Engineering (ESCMSE)

Journal of Numerical Analysis, Industrial and Applied Mathematics (JNAIAM)
vol. 14, no. 3-4, 2020, pp. 1-15
ISSN 1790–8140

Numerical approximations of the Keyfitz-Kranzer type models by using entropy stable schemes

Carlos A. Vega[1]
Departmento de Matemáticas y Estadística,
Universidad del Norte,
Km 5 Via Puerto Colombia Barranquilla, Colombia.

Sonia Valbuena
Grupo GIHEM,
Universidad del Atlántico,
Km 7 Via Puerto Colombia Barranquilla, Colombia.

Abstract: Numerical simulations for the Keyfitz-Kranzer system of equations are developed by using high-order entropy stable schemes proposed by Fjordholm et. al. [Arbitrary high-order essentially non-oscillatory entropy stable schemes for systems of conservation laws, SIAM J. Numer. Anal., **50**, 544-573 (2012)]. Since existence of entropy pairs is an important ingredient to this approach, they are described in details. Numerical experiments include errors and convergence rates to illustrate the performance of the schemes.

Keywords: Conservation laws, Keyfitz-Kranzer system, entropy conservative flux, entropy stable scheme.

Mathematics Subject Classification: 35L65, 35L45, 35L67, 58J45, 65M06

1 Introduction

We consider the Keyfitz-Kranzer system of equations

$$\boldsymbol{u}_t + (\phi(r)\boldsymbol{u})_x = 0, \qquad x \in \mathbb{R}, \quad t > 0, \tag{1}$$

where $\boldsymbol{u} = (u_1, \ldots, u_n)^T$ is the unknown vector, $r = |u_1|^m + \cdots + |u_n|^m = \|\boldsymbol{u}\|_m^m$ for any $m \in \mathbb{Z}^+$ fixed and $\phi \in C^1(\mathbb{R}_+)$ is a scalar function with

$$r\phi(r) \to 0 \quad \text{as} \quad r \to 0+. \tag{2}$$

A straighforward computation shows that the entries of Jacobian matrix $A(\boldsymbol{u}) := \boldsymbol{f}_{\boldsymbol{u}}(\boldsymbol{u})$ of the flux function $\boldsymbol{f}(\boldsymbol{u}) = \phi(r)\boldsymbol{u}$ are given by

[1]E-mail: cvega@uninorte.edu.co

$$A_{i,j} = \phi(r)\delta_{i,j} + m\phi'(r)u_i u_j |u_j|^{m-2}, \quad i,j = 1,\dots,n \quad \text{and } m \geq 2$$

where $\delta_{i,j}$ is the Kronecker delta. When $m = 1$ and $u_i \geq 0$, $i = 1,\dots,n$,

$$A_{i,j} = \phi(r)\delta_{i,j} + \phi'(r)u_i, \quad i,j = 1,\dots,n.$$

In either case, $A(\boldsymbol{u})$ can be viewed as a rank-one perturbation of the diagonal matrix $\phi(r)I$, namely

$$A(\boldsymbol{u}) = \phi(r)I + m\phi'(r)\boldsymbol{u}\boldsymbol{w}^T,$$

where $\boldsymbol{w}^T = (u_1|u_1|^{m-2},\dots,u_n|u_n|^{m-2})$ and I denotes the $n \times n$ identity matrix. For $m = 2$ the matrix $A(\boldsymbol{u})$ is symmetric, therefore the system (1) is hyperbolic. The same conclusion can be easily drawn for $m \neq 2$. First, note that the eigenvalues of $A(\boldsymbol{u})$ are $\lambda_1(\boldsymbol{u}) = \phi(r)$ with algebraic multiplicity $n-1$ and $\lambda_2(\boldsymbol{u}) = \phi(r) + mr\phi'(r)$ with algebraic multiplicity 1 and corresponding eigenvector $\boldsymbol{u}$. If $\boldsymbol{u} \neq 0$, the eigenspace $span\{\boldsymbol{w}\}^{\perp}$ corresponding to the first eigenvalue has dimension $n-1$, then $\lambda_1(\boldsymbol{u})$ has geometric multiplicity $n-1$, it follows that the geometric and algebraic multiplicities of each eigenvalue are equal. Therefore, $A(\boldsymbol{u})$ is diagonalizable. Due to the existence of repeated eigenvalues, the system (1) is nonstrictly hyperbolic when $n > 2$.
The system (1) was originally proposed by B. L. Keyfitz and H. C. Kranzer in [13] as a model to describe the propagation of longitudinal and transverse waves in a stretched elastic string. This system arises in a wide variety of problems, including magnetohydrodynamics, where it is used to investigate some features of solar wind [3], enhance oil recovery and modeling polymer flooding in porous media [25]. Another interesting example is the well-known $n \times n$ chromatography system of conservation laws [1]:

$$\boldsymbol{u}_t + \left(\frac{\boldsymbol{u}}{1 + \sum_{i=1}^{n} u_i}\right)_x = 0, \quad u_i \geq 0, \quad i = 1,\dots,n, \tag{3}$$

which can be obtained from (1) by taking $m = 1$ and $\phi(r) = 1/(1+r)$ with $r = u_1 + \cdots + u_n$.
The existence and uniqueness of strong generalized entropy solution to the Cauchy problem for (1) with initial data $\boldsymbol{u}_0 \in L^{\infty}(\mathbb{R},\mathbb{R}^n)$ was proved by E. Y. Panov in [17], where besides, a set of entropies of the system is provided. The last-mentioned author also proved that the theory of strong generalized entropy solutions also holds when $\boldsymbol{u}_0 \in L^{\infty}(\mathbb{R},X)$, X being an arbitrary real Banach space (see [18]).
Numerical studies of system (1) for the particular case where $m = 2$ have been conducted in [14] and [19] by using an upwind finite difference scheme and the front tracking method, respectively.
The rest of the paper is organized as follow. Section 2 is devoted to present entropy pairs and entropy potential functions in explicit forms. In Section 3, we briefly review theory about entropy conservative and entropy stable schemes described in [6, 23]. In Section 4 numerical experiments are provided. In Section 5 some conclusions are drawn.

2 Entropy pair for the Keyfitz-Kranzer system

Let us first recall that a convex scalar function $E = E(\boldsymbol{u}) \in C^1$ is an entropy for the system of conservation laws

$$\boldsymbol{u}_t + \boldsymbol{f}(\boldsymbol{u})_x = 0, \tag{4}$$

with associated entropy flux $Q = Q(\boldsymbol{u})$ if

$$\nabla_{\boldsymbol{u}} Q(\boldsymbol{u}) = \boldsymbol{v}^{\mathrm{T}} A(\boldsymbol{u}), \tag{5}$$

where

$$\boldsymbol{v} = \nabla E(\boldsymbol{u}) = \big(\partial_{u_1} E(\boldsymbol{u}), \ldots, \partial_{u_n} E(\boldsymbol{u})\big)^{\mathrm{T}}$$

is the vector of entropy variables. (E, Q) is called an entropy pair for the conservation law (1). When E is strictly convex, the entropy variables $\boldsymbol{v}$ symmetrize the (4) by making the change of variables $\boldsymbol{u} = \boldsymbol{u}(\boldsymbol{v})$ [16], which puts the system (4) into its equivalent symmetric form

$$\boldsymbol{u}(\boldsymbol{v})_t + \boldsymbol{g}(\boldsymbol{v})_x = 0, \quad \boldsymbol{g}(\boldsymbol{v}) := \boldsymbol{f}(\boldsymbol{u}(\boldsymbol{v})). \tag{6}$$

Note that the Jacobian of $\boldsymbol{g}(\boldsymbol{v})$ is the Hessian of the function

$$\psi(\boldsymbol{v}) := \boldsymbol{v}^{\mathrm{T}} \boldsymbol{f}(\boldsymbol{u}(\boldsymbol{v})) - Q(\boldsymbol{u}(\boldsymbol{v})). \tag{7}$$

The function ψ is called entropy potential and plays an important role in the construction of entropy conservative fluxes.
A system of conservation laws (4) endowed with an entropy pair satisfies the additional conservation law

$$\partial_t E(\boldsymbol{u}) + \partial_x Q(\boldsymbol{u}) = 0, \tag{8}$$

for smooth solutions. However, it is well known that solutions of (4) develop discontinuities, therefore the entropy equation (8) transforms into the entropy inequality

$$\partial_t E(\boldsymbol{u}) + \partial_x Q(\boldsymbol{u}) \leq 0 \tag{9}$$

in the sense of distributions. The entropy condition (9) single out a unique solution and it is useful to obtain a priori L^p-stability bounds.
Our next claim is to provide an explicit entropy pair for (1) with the corresponding entropy potential. The set of entropies of the system (1) has been described in [17] (see Theorem 1). It is worth pointing out that in the last-mentioned reference the function $E(\boldsymbol{u})$ belongs to $C^1(\mathbb{R}^n \setminus \{0\})$ satisfying the Lipschitz condition in a neighbourhood of the origin and the gradient $\nabla E(\boldsymbol{u})$ at the origin is defined by $\nabla E(0) = 0$. In [11], the following two explicit entropy pairs of system (1) were used for obtaining convergence results when $n = 2$ and $m > 1$,

$$(E, Q) = \left(r, \int^r (\phi(s) + ms\phi'(s))\, ds\right) \tag{10}$$

$$(E, Q) = \left(\int^r (\phi(s) + ms\phi'(s))\, ds, \int^r (\phi(s) + ms\phi'(s))^2\, ds\right) \tag{11}$$

For arbitrary n and $m > 1$ the entropy function in (10) can be obtained directly as follow. Assume that $E(\boldsymbol{u})$ is an additively separable function, that is, $E(\boldsymbol{u}) = e_1(u_1) + \cdots + e_n(u_n)$. Then the Hessian of E is a diagonal matrix. Now, it is fairly easy to see that $E_{\boldsymbol{uu}}(\boldsymbol{u})A(\boldsymbol{u})$ is symmetric if

$$e_i''(u_i) = |u_i|^{m-2}, \quad i = 1, \ldots, n$$

Therefore, for n arbitrary and $m > 1$

$$E(\boldsymbol{u}) = \frac{1}{m(m-1)} \sum_{i=1}^{n} |u_i|^m = \frac{r}{m(m-1)}, \tag{12}$$

is an entropy function of the system (1) with entropy flux

$$Q(\boldsymbol{u}) = \frac{1}{m(m-1)} \int^r (\phi(s) + ms\phi'(s))\, ds. \tag{13}$$

Note that for $m = 2$, $E(\boldsymbol{u}) = \frac{1}{2}\sum_{i=1}^{n} u_i^2$ which coincide with the standard entropy function for symmetric systems.
The entropy pair (12)-(13) leads to the entropy potential

$$\psi(\boldsymbol{u}) = \frac{1}{m}\int^{r} \phi(s)\, ds. \tag{14}$$

In the case $m = 1$ with $u_i \geq 0$, $i = 1, \ldots, n$, (1) reduces to an analogue system of the so called multi-class Lighthill-Whitham-Richards traffic model [2]. In the last-mentioned reference (see Proposition 2.1) the following entropy pair is provided by assuming that $u_i > 0$, $i = 1, \ldots, n$:

$$E(\boldsymbol{u}) = \sum_{i=1}^{n} u_i(\ln u_i - 1), \quad Q(\boldsymbol{u}) = \phi(r)\sum_{i=1}^{n} u_i \ln u_i - \Phi(r),$$

where the function Φ is any primitive of ϕ. The corresponding entropy variables are

$$\boldsymbol{v} = (\ln u_1, \ldots, \ln u_n)^{\mathrm{T}}, \tag{15}$$

and the entropy potential is given by

$$\psi(\boldsymbol{u}) = (\ln u_1, \ldots, \ln u_n)\,\phi(r)\begin{pmatrix} u_1 \\ \vdots \\ u_n \end{pmatrix} - \phi(r)\sum_{i=1}^{n} u_i \ln u_i + \Phi(r) = \Phi(r).$$

3 Entropy stable and entropy conservative numerical schemes

A semi-discrete conservative and consistent scheme for (4) on a uniform spatial mesh $x_j = j\Delta x$, $j \in \mathbb{Z}$ is given by

$$\frac{\mathrm{d}\boldsymbol{u}_j(t)}{\mathrm{d}t} = -\frac{1}{\Delta x}\left(\boldsymbol{F}_{j+1/2} - \boldsymbol{F}_{j-1/2}\right), \quad j \in \mathbb{Z}, \tag{16}$$

where $\boldsymbol{u}_j(t)$ denotes the numerical approximation of $\boldsymbol{u}(x_j, t)$ and

$$\boldsymbol{F}_{j+1/2} = \boldsymbol{F}(\boldsymbol{u}_{j-p+1}, \ldots, \boldsymbol{u}_{j+p})$$

is the numerical flux associated with $x_{j+1/2}$. We assume that $\boldsymbol{F}_{j+1/2}$ is a Lipschitz continuous function and consistent with the differential flux in the standard sense, *i.e.* $\boldsymbol{F}(\boldsymbol{u}, \boldsymbol{u}, \ldots, \boldsymbol{u}) = \boldsymbol{f}(\boldsymbol{u})$. The scheme (16) is called *entropy stable* with respect to the entropy pair (E, Q) if it satisfies a discrete entropy inequality

$$\frac{\mathrm{d}}{\mathrm{d}t}E(\boldsymbol{u}_j(t)) + \frac{1}{\Delta x}\left(\tilde{Q}_{j+1/2} - \tilde{Q}_{j-1/2}\right) \leq 0 \tag{17}$$

for some *numerical entropy flux* $\tilde{Q}_{j+1/2}$ consistent with the entropy flux Q. If equality holds in (17), then the scheme (16) is called *entropy conservative*.
Let us recall a basic result related to the design of an entropy preserving numerical flux. First we introduce the notation

$$[\![a]\!]_{j+1/2} := a_{j+1} - a_j, \qquad \overline{a}_{j+1/2} := \frac{1}{2}(a_{j+1} + a_j).$$

Theorem 3.1 (Tadmor [23]) *Assume that the one-dimensional system of conservation laws* (4) *is endowed with an entropy pair* (E, Q). *Suppose that* $\tilde{\boldsymbol{F}}_{j+1/2}$ *is a consistent numerical flux that satisfies*

$$[\![\boldsymbol{v}]\!]_{j+1/2}^{\mathrm{T}} \tilde{\boldsymbol{F}}_{j+1/2} = [\![\psi]\!]_{j+1/2}, \quad j \in \mathbb{Z}. \tag{18}$$

Then the conservative scheme

$$\frac{\mathrm{d}\boldsymbol{u}_j(t)}{\mathrm{d}t} = -\frac{1}{\Delta x}\left(\tilde{\boldsymbol{F}}_{j+1/2} - \tilde{\boldsymbol{F}}_{j-1/2}\right), \quad j \in \mathbb{Z},$$

is second-order accurate and entropy conservative, and satisfies the discrete entropy identity

$$\frac{\mathrm{d}}{\mathrm{d}t}E(\boldsymbol{u}_j(t)) = -\frac{1}{\Delta x}\left(\tilde{Q}_{j+1/2} - \tilde{Q}_{j-1/2}\right), \quad j \in \mathbb{Z},$$

with the numerical entropy flux $\tilde{Q}_{j+1/2} = \bar{\boldsymbol{v}}_{j+1/2}^{\mathrm{T}} \tilde{\boldsymbol{F}}_{j+1/2} - \bar{\psi}_{j+1/2}$.

According to Theorem 3.1, the existence of an explicitly given entropy pair is an important ingredient in designing entropy conservative schemes. For the scalar case, the solution of (18) is unique. However, for systems of conservation laws this is no longer true, since the condition (18) provides a single algebraic equation for several unknowns. In [24], Tadmor proposed the following general solution of (18):

$$\tilde{\boldsymbol{F}}_{j+1/2} = \int_{-1/2}^{1/2} \boldsymbol{f}\big(\boldsymbol{v}_{j+1/2}(\xi)\big)\,\mathrm{d}\xi, \tag{19}$$

where $\boldsymbol{v}_{j+1/2}(\xi)$ denotes the straight line connecting $\boldsymbol{v}_j$ and $\boldsymbol{v}_{j+1}$, i.e.,

$$\boldsymbol{v}_{j+1/2}(\xi) = \frac{1}{2}(\boldsymbol{v}_j + \boldsymbol{v}_{j+1}) + \xi(\boldsymbol{v}_{j+1} - \boldsymbol{v}_j), \qquad \xi \in [-1/2, 1/2].$$

The flux (19) is sometimes called Averaged Energy Conservative (AEC for short) flux [8]. In [24], Tadmor also constructed an explicit solution of (18) based on different paths in the phase space of the entropy variables. The procedure described by Tadmor is as follows: Let $\{\boldsymbol{r}_i\}_{i=1}^n$ be an arbitrary set of n linearly independent vectors, and let $\{\boldsymbol{l}_i\}_{i=1}^n$ be the corresponding orthogonal set. At an interface $x_{j+1/2}$, we define the paths

$$\boldsymbol{v}^0 := \boldsymbol{v}_j, \quad \boldsymbol{v}^i := \boldsymbol{v}^{i-1} + \big([\![\boldsymbol{v}]\!]_{j+1/2}^{\mathrm{T}} \boldsymbol{l}_i\big)\boldsymbol{r}_i \quad \text{for } i = 1, \ldots, n-1, \quad \boldsymbol{v}^n := \boldsymbol{v}_{j+1}.$$

Then the entropy conservative flux is given by

$$\tilde{\boldsymbol{F}}_{j+1/2} = \sum_{i=1}^{n} \frac{\psi(\boldsymbol{v}^i) - \psi(\boldsymbol{v}^{i-1})}{[\![\boldsymbol{v}]\!]_{j+1/2}^{\mathrm{T}} \boldsymbol{l}_i}\, \boldsymbol{l}_i. \tag{20}$$

This flux is termed the Pathwise Energy Conservative (PEC) flux.

The two-point entropy conservative fluxes described above are only second-order accurate. However, LeFloch et al. [15] proposed a procedure to construct $2p$-th order entropy conservative fluxes by linear combinations of two-point entropy conservative fluxes $\tilde{\boldsymbol{F}}$. For instance, the fourth-order entropy conservative flux corresponding to $p = 2$, which will be used in numerical examples, is given by

$$\tilde{\boldsymbol{F}}_{j+1/2}^4 = \frac{4}{3}\tilde{\boldsymbol{F}}(\boldsymbol{u}_j, \boldsymbol{u}_{j+1}) - \frac{1}{6}\big(\tilde{\boldsymbol{F}}(\boldsymbol{u}_{j-1}, \boldsymbol{u}_{j+1}) + \tilde{\boldsymbol{F}}(\boldsymbol{u}_j, \boldsymbol{u}_{j+2})\big). \tag{21}$$

Entropy conservative schemes perform well in smooth regions. But they produce high-frequency oscillations closed to discontinuities. Therefore, it is necessary to add suitable numerical diffusion

to guarantee that entropy is dissipated. To this end, we used the higher-order numerical diffusion operator designed by Fjordholm et al [6]. In the last-mentioned reference, the numerical flux is defined as

$$\boldsymbol{F}_{j+1/2} = \tilde{\boldsymbol{F}}^4_{j+1/2} - \frac{1}{2}\boldsymbol{D}_{j+1/2}\langle\!\langle \boldsymbol{v} \rangle\!\rangle_{j+1/2}, \tag{22}$$

where $\langle\!\langle \boldsymbol{v} \rangle\!\rangle_{j+1/2}$ is the difference in the reconstructed states, that is,

$$\langle\!\langle \boldsymbol{v} \rangle\!\rangle_{j+1/2} := \boldsymbol{s}_{j+1}(x_{j+1/2}) - \boldsymbol{s}_j(x_{j+1/2}) \tag{23}$$

for some reconstructed function $\boldsymbol{s}_j(x)$ which will be specified later, and $\boldsymbol{D}_{j+1/2}$ is a diffusion matrix of the form

$$\boldsymbol{D}_{j+1/2} = \boldsymbol{R}_{j+1/2}\boldsymbol{\Lambda}_{j+1/2}\boldsymbol{R}^{\mathrm{T}}_{j+1/2}. \tag{24}$$

Here, $\boldsymbol{R}_{j+1/2}$ is the matrix of right eigenvectors of the flux Jacobian $A(\boldsymbol{u}_{j+1/2})$ with $\boldsymbol{u}_{j+1/2} := (\boldsymbol{u}_j + \boldsymbol{u}_{j+1})/2$ and $\boldsymbol{\Lambda}_{j+1/2}$ is a positive diagonal matrix that depends on the eigenvalues of the flux Jacobian. In this work, we use the Rusanov-type diffusion operator.

$$\boldsymbol{\Lambda}_{j+1/2} = \max\big\{|\lambda_1|, |\lambda_2|, \ldots, |\lambda_n|\big\}\boldsymbol{I},$$

where $\boldsymbol{I}$ is the $n \times n$ identity matrix. The following lemma provides sufficient conditions to ensure entropy stability of the scheme with numerical flux (22).

Lemma 3.1 (Fjordholm et al. [6]) *For each $j \in \mathbb{Z}$, let $\boldsymbol{D}_{j+1/2}$ given by* (24)*. Let $\boldsymbol{s}_j(x)$ be a polynomial reconstruction of the entropy variable in the cell I_j such that for each j, there exists a diagonal matrix $\boldsymbol{B}_{j+1/2} \geq 0$ such that*

$$\langle\!\langle \boldsymbol{v} \rangle\!\rangle_{j+1/2} = \big(\boldsymbol{R}^{\mathrm{T}}_{j+1/2}\big)^{-1}\boldsymbol{B}_{j+1/2}\boldsymbol{R}^{\mathrm{T}}_{j+1/2}[\![\boldsymbol{v}]\!]_{j+1/2} \tag{25}$$

Then the scheme with numerical flux (22) *is entropy stable.*

By introducing the *scaled entropy variables*

$$\mathbf{w}^{\pm}_j := \boldsymbol{R}^{\mathrm{T}}_{j\pm1/2}\boldsymbol{v}_j, \qquad \tilde{\boldsymbol{w}}^{\pm}_j := \boldsymbol{R}^{\mathrm{T}}_{j\pm1/2}\boldsymbol{v}^{\pm}_j, \tag{26}$$

with the reconstructed entropy variables

$$\boldsymbol{v}^{+}_j = \boldsymbol{s}_j(x_{j+1/2}), \qquad \boldsymbol{v}^{-}_j = \boldsymbol{s}_j(x_{j-1/2}), \tag{27}$$

the condition (25) can be expressed as

$$\langle\!\langle \tilde{\boldsymbol{w}} \rangle\!\rangle_{j+1/2} = \boldsymbol{B}_{j+1/2}\langle\!\langle \boldsymbol{w} \rangle\!\rangle_{j+1/2}. \tag{28}$$

Denoting the l-th component of $\boldsymbol{w}_j$ and $\tilde{\boldsymbol{w}}_j$ by w^l_j and $\tilde{w}^l_j$, respectively, the condition (28) is equivalent to the so-called *sign property*:

$$sign\langle\!\langle \tilde{w}^l_j \rangle\!\rangle_{j+1/2} = sign\langle\!\langle w^l_j \rangle\!\rangle_{j+1/2}. \tag{29}$$

The sign property states that the jump of the reconstructed point values at each cell interface has the same sign as the jump of the underlying point values across that interface. The reconstruction procedure of the scaled entropy variables that satisfy the sign property is carried out as follows (see [6, Corollary 3.5]). Given the interface values of each component $w = w^l$ of the scaled entropy variables $\boldsymbol{w}$ for a fix grid cell I_j, we define the point value $\mu^j_j := w^-_j$, and inductively

$$\mu^j_{i+1} := \mu^j_i + \delta_{i+1/2}, \quad i = j, j+1, \ldots; \quad \mu^j_{i-1} := \mu^j_i - \delta_{i+1/2}, \quad i = j, j-1, \ldots,$$

where $\delta_{i+1/2} = \langle\!\langle w \rangle\!\rangle_{i+1/2}$. Similarly, we define $\nu_j^j := w_j^+$ and

$$\nu_{i+1}^j := \nu_i^j + \delta_{i+1/2}, \quad i = j, j+1, \ldots; \quad \nu_{i-1}^j := \nu_i^j - \delta_{i+1/2}, \quad i = j, j-1, \ldots.$$

Let $\Upsilon_i^j(x) := \mathcal{R}_i(\{\mu_k^j\}_{k\in\mathbb{Z}})$ and $\Psi_i^j(x) := \mathcal{R}_i(\{\nu_k^j\}_{k\in\mathbb{Z}})$ be the reconstructions of μ^j and ν^j in cell I_i. Then the left and right reconstructed values are

$$\tilde{w}_j^- := \Upsilon_j^j(x_{j-1/2}) \quad \text{and} \quad \tilde{w}_j^+ := \Psi_j^j(x_{j+1/2})$$

Since (26) implies that $\boldsymbol{v}_j^\pm := (\boldsymbol{R}_{j\pm1/2}^{\mathrm{T}})^{-1}\tilde{\boldsymbol{w}}_j^\pm$, the diffusion term $\boldsymbol{D}_{j+1/2}\langle\!\langle \boldsymbol{v} \rangle\!\rangle_{j+1/2}$ can be expressed as

$$\begin{aligned}\boldsymbol{D}_{j+1/2}\langle\!\langle \boldsymbol{v} \rangle\!\rangle_{j+1/2} &= \boldsymbol{R}_{j+1/2}\boldsymbol{\Lambda}_{j+1/2}\boldsymbol{R}_{j+1/2}^{\mathrm{T}}\big(\boldsymbol{R}_{j+1/2}^{\mathrm{T}}\big)^{-1}\langle\!\langle \tilde{\boldsymbol{w}} \rangle\!\rangle_{j+1/2} \\ &= \boldsymbol{R}_{j+1/2}\boldsymbol{\Lambda}_{j+1/2}\langle\!\langle \tilde{\boldsymbol{w}} \rangle\!\rangle_{j+1/2}\end{aligned}$$

Thus, it is not necessary to compute the inverse of $\boldsymbol{R}_{j+1/2}^{\mathrm{T}}$ for each j to recover $\boldsymbol{v}_j^\pm$. Fjordholm et al. proved that ENO method satisfies the sign property [7] and designed a class of arbitrary high-order entropy stable schemes (TeCNO schemes) [6]. In this paper, we combine the fourth-order entropy conservative flux (21) with a numerical diffusion term based on fourth-order ENO reconstruction of the scaled entropy variables, labeled TeCNO4 in the last-mentioned reference.
We briefly mention some others reconstruction procedures that satisfy the sign property. Fjordholm and Ray [9] developed a third-order WENO reconstruction method (SP-WENO3 for short) that satisfies the property (the standard WENO methods fail to satisfy the sign property.). In [4], Cheng and Nie proposed a third-order entropy stable based on a non-oscillatory piecewise-quadratic reconstruction from point values and more recently, the former author developed a new fourth order non-oscillatory reconstruction procedure which satisfies the sign property [5].

Time discretization
To complete the computation of the semi-discrete framework (16) maintaining high order in time and simplicity, the popular explicit three-stage third-order *strong stability preserving* Runge-Kutta method SSPRK(3,3) will be used [10]. This method is given by the steps

$$\begin{aligned}\boldsymbol{u}^{(1)} &= \boldsymbol{u}^\nu + \Delta t\boldsymbol{\mathcal{L}}\big(\boldsymbol{u}^\nu\big), \\ \boldsymbol{u}^{(2)} &= \frac{3}{4}\boldsymbol{u}^\nu + \frac{1}{4}\boldsymbol{u}^{(1)} + \frac{1}{4}\Delta t\boldsymbol{\mathcal{L}}\big(\boldsymbol{u}^{(1)}\big), \\ \boldsymbol{u}^{\nu+1} &= \frac{1}{3}\boldsymbol{u}^\nu + \frac{2}{3}\boldsymbol{u}^{(2)} + \frac{2}{3}\Delta t\boldsymbol{\mathcal{L}}\big(\boldsymbol{u}^{(2)}\big),\end{aligned}$$

where

$$[\mathcal{L}(\boldsymbol{u})]_j := -\frac{1}{\Delta x}\big(\boldsymbol{F}_{j+1/2} - \boldsymbol{F}_{j-1/2}\big).$$

In order to guarantee that the explicit scheme obtained to be stable, the time and space discretization steps must obey the CFL condition. For this purpose, the value of Δt is computed adaptively for each step ν. More exactly, the solution $\boldsymbol{u}^{\nu+1}$ at $t_{\nu+1} = t_\nu + \Delta t$ is calculated from $\boldsymbol{u}^\nu$ by using the time step $\Delta t = \mathrm{CFL}\Delta x/\alpha_{\max}^n$, where $\alpha_{\max}^\nu$ is an estimate of the maximal characteristic velocity for $\boldsymbol{u}^\nu$. All numerical experiments are carried out with a CFL number of 0.4.

4 Numerical experiments

In this section, several numerical examples are presented for 2×2 Keyfitz-Kranzer system with different values of m. Numerical results include errors in L^1 norm and orders of convergence. Let

$u^N_{i,\cdot}(t)$ denote the approximate solution for the i-th component at time t and $\Delta x = (b-a)/N$. Then the L^1 error for the i-th component is computed as follows

$$e_i = e_i(t) = \left\| u_i(\cdot,t) - u^N_{i,\cdot}(t) \right\|_1 = \Delta x \sum_{j=1}^{N} \left| u_i(x_j,t) - u^N_{i,j}(t) \right|,$$

where $u_i(\cdot,t)$ is the i-th component of the exact solution if available (Examples 4.2 and 4.3) or a reference solution (Example 4.1), that is, a numerical solution computed on a fine spatial mesh. Here, we use the well-known fifth order WENO method with 6400 grid points as reference solution. Besides errors, we also include for each example an estimation of the convergence rate which is computed by the standard formula

$$cr = \frac{log(e(N_2)/e(N_1))}{log(N_1/N_2)}, \tag{30}$$

where $e(N_1)$ and $e(N_2)$ are the errors associated with the consecutive values of N, N_1 and N_2.
In the first example (symmetric Keyfitz-Kranzer system) numerical solutions are computed by using the PEC flux in (22). However, for $m \neq 2$ the PEC flux seems to be numerically unstable (similar problems for the shallow water equations are reported in [8]). On the other hand, it is not possible to express the path integral (19) in closed form for the chromatography system. Therefore, numerical solutions for Examples 4.2 and 4.3 are computed by approximating the integral (19) with adaptive Simpson quadrature.
Recall that numerical solutions are computed by the entropy stable scheme based on fourth-order ENO reconstruction along with the three-stage third-order Runge-Kutta time discretization method. It is worth pointing out that the scheme will be fourth-order accurate where solutions are smooth. However, the solutions of examples presented here contain shocks or contact discontinuity. Then, the only purpose of displaying convergence rates is to illustrate the behavior of the approximate solutions with different discretizations.

Example 4.1 *This example is taken from [19]. Consider the* 2×2 *system* (1) *with* $r = |u_1|^2+|u_2|^2$, $\phi(r) = r - 4\sqrt{r} + 5.5$ *and the following initial data*

$$\boldsymbol{u}(x,0) = (\sin(\pi x) + 1.5) \begin{pmatrix} \sin(\pi x) \\ \cos(\pi x) \end{pmatrix}, \qquad x \in [-1,1],$$

with periodic boundary conditions.
The entropy potential is

$$\psi(\boldsymbol{u}) = \frac{1}{4} r^2 - \frac{4}{3} r^{3/2} + \frac{5.5}{2} r$$

which follows from (14). *In this example, the approximate solution is computed by using the PEC flux which involves an intensive usage of the characteristic information. Specifically, the right eigenvectors*

$$\boldsymbol{r}_1 = \frac{1}{\|\boldsymbol{u}\|_2} (-u_2, u_1)^{\mathrm{T}}, \quad \boldsymbol{r}_2 = \frac{1}{\|\boldsymbol{u}\|_2} \boldsymbol{u}$$

with the corresponding orthogonal set of left eigenvectors $\boldsymbol{l}_1 = \boldsymbol{r}_1$ *and* $\boldsymbol{l}_2 = \boldsymbol{r}_2$. *The errors in* L^1 *norm* ($\times 10^{-3}$) *and orders of convergence for each component for* $t = 0.5$ *and* $t = 0.75$ *are shown in Table 1. It can be seen that the convergence rate is approximately equal to* 1. *Figures 1 and 2 show the performance of the entropy stable flux described by* (20)-(21)-(22) *at* $t = 0.5$ *and* $t = 0.75$ *with* 200 *grids. A small glitch can be observed at the beginning and at the end of the domain. However, this phenomenom disappears as the mesh is refined.*

	$t = 0.5$				$t = 0.75$			
	u_1		u_2		u_1		u_2	
N	e_1	cr	e_2	cr	e_1	cr	e_2	cr
100	189.64	—	177.29	—	330.35	—	245.64	—
200	77.38	1.293	80.81	1.133	136.88	1.271	104.69	1.230
400	37.70	1.038	41.55	0.960	65.16	1.071	50.45	1.053
800	16.36	1.204	18.44	1.172	27.56	1.242	21.12	1.256
1600	7.64	1.098	8.64	1.094	12.36	1.156	9.59	1.139

Table 1: Example 4.1: approximate L^1-errors ($\times 10^{-3}$) and convergence rates.

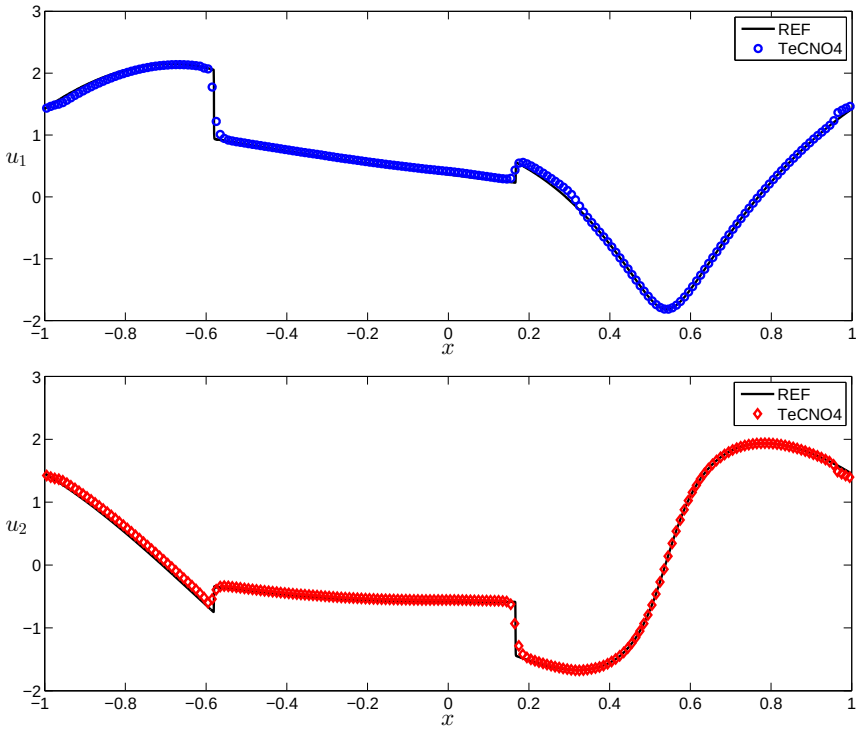

Figure 1: Example 4.1 : Approximate solutions at $t = 0.5$ with $N = 200$ grid points corresponding to the first component (top) and the second component (bottom).

Example 4.2 *Let us consider the system of Keyfitz-Kranzer with* $m = 3$ *and* $u_1 \geq 0$ *and* $u_2 \geq 0$. *Under these assumptions,* $r = u_1^3 + u_2^3$ *and*

$$\boldsymbol{r}_1 = (-u_2^2, u_1^2)^{\mathrm{T}}, \quad \boldsymbol{r}_2 = \boldsymbol{u}$$

The solution of this problem was obtained in [26] subject to the Riemann initial data

$$\boldsymbol{u}(x,0) = \begin{cases} \boldsymbol{u}_-, & x < 0, \\ \boldsymbol{u}_+, & x > 0. \end{cases} \tag{31}$$

Here, we take $\boldsymbol{u}_- = (0.5, 1.5)^{\mathrm{T}}$, $\boldsymbol{u}_+ = (1.5, 2.0)^{\mathrm{T}}$. *In order to obtain the exact solution in fully*

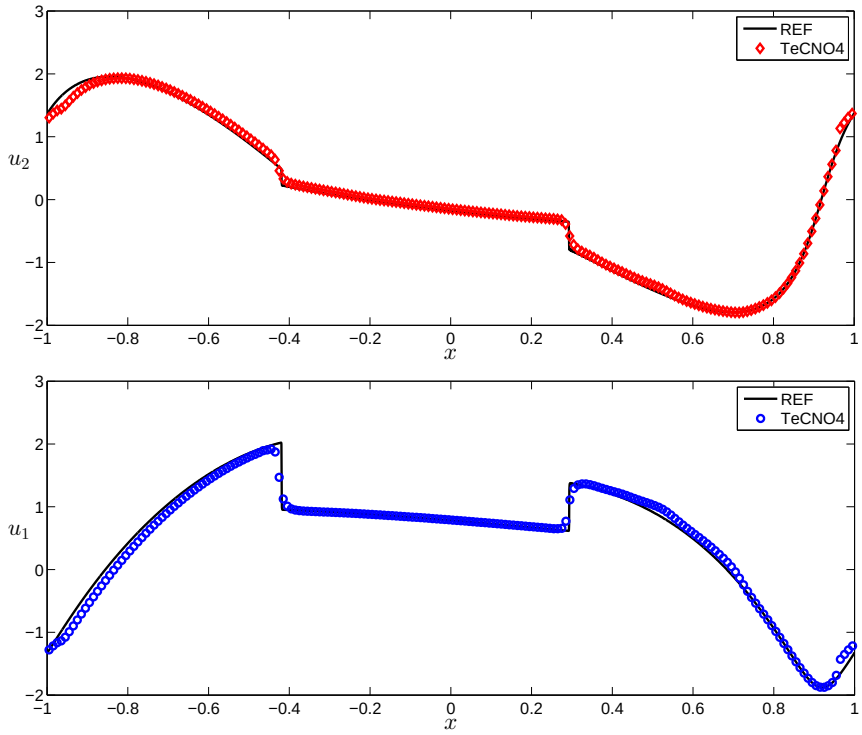

Figure 2: Example 4.1 : Approximate solutions at $t = 0.75$ with $N = 200$ grid points corresponding to the first component (top) and the second component (bottom).

explicit forms, we take the simple expression $\phi(r) = r$.
Writing $r_- = \|\boldsymbol{u}_-\|_3^3$ *and* $r_+ = \|\boldsymbol{u}_+\|_3^3$, *the exact solution is given by (see [26] for more details)*

$$\boldsymbol{u}(x,t) = \begin{cases} \boldsymbol{u}_-, & x < \tau_1 t, \\ \boldsymbol{u}_*, & \tau_1 t < x < \lambda_2(\boldsymbol{u}_-)t, \\ \widehat{\boldsymbol{u}}(x/t), & \lambda_2(\boldsymbol{u}_-)t \le x \le \lambda_2(\boldsymbol{u}_+)t, \\ \boldsymbol{u}_+, & x > \lambda_2(\boldsymbol{u}_+)t, \end{cases} \tag{32}$$

where the intermediate state $\boldsymbol{u}_*$ *is calculated by* $\boldsymbol{u}_* = \frac{\|\boldsymbol{u}_-\|_3}{\|\boldsymbol{u}_+\|_3}\boldsymbol{u}_+$, *and* $\tau_1 = \phi(r_-)$. *The state* $\widehat{\boldsymbol{u}}(x/t)$ *in the rarefaction wave corresponding to* λ_2 *varies from* $\boldsymbol{u}_*$ *to* $\boldsymbol{u}_+$, *which can be determined uniquely by*

$$\frac{u_1}{u_2} = \frac{u_{1,-}}{u_{2,-}}, \quad \xi = \phi(r) + mr\phi'(r), \tag{33}$$

where $u_{1,-}$ *and* $u_{2,-}$ *are the components of* $\boldsymbol{u}_-$. *Since* $\widehat{\boldsymbol{u}}$ *satisfies*

$$\widehat{\boldsymbol{u}}'(\xi) = \frac{\boldsymbol{r}_2(\boldsymbol{u})}{\nabla\lambda_2(\boldsymbol{u})\cdot\boldsymbol{r}_2(\boldsymbol{u})} = \frac{\boldsymbol{u}}{mr((m+1)\phi'(r) + mr\phi''(r))} = \frac{\boldsymbol{u}}{mr(m+1)}, \tag{34}$$

with $\xi = x/t$, *and taking into account* (33), *it follows that*

$$\widehat{\boldsymbol{u}}(\xi) = \sqrt[m]{\frac{\xi - \xi_-}{(m+1)(\kappa^m+1)} + u_{1,-}}\begin{pmatrix}1\\ \kappa\end{pmatrix}, \tag{35}$$

with $\kappa = \frac{u_{1,-}}{u_{2,-}}$. *The approximate solutions at* $t = 0.5$ *and* $t = 1$ *on a mesh of 200 points are shown in Figures 3 and 4. Errors and convergence rates are presented in Table 2.*

	$t = 0.5$				$t = 1$			
	u_1		u_2		u_1		u_2	
N	e_1	cr	e_2	cr	e_1	cr	e_2	cr
100	269.19	—	150.95	—	298.42	—	119.85	—
200	129.66	1.054	78.38	0.946	118.16	1.337	52.13	1.201
400	66.01	0.974	32.48	1.271	70.71	0.741	28.09	0.892
800	39.39	0.745	17.65	0.880	41.20	0.780	17.46	0.686
1600	24.05	0.712	10.53	0.745	25.18	0.710	10.05	0.797

Table 2: Example 4.2: approximate L^1-errors ($\times 10^{-3}$) and convergence rates.

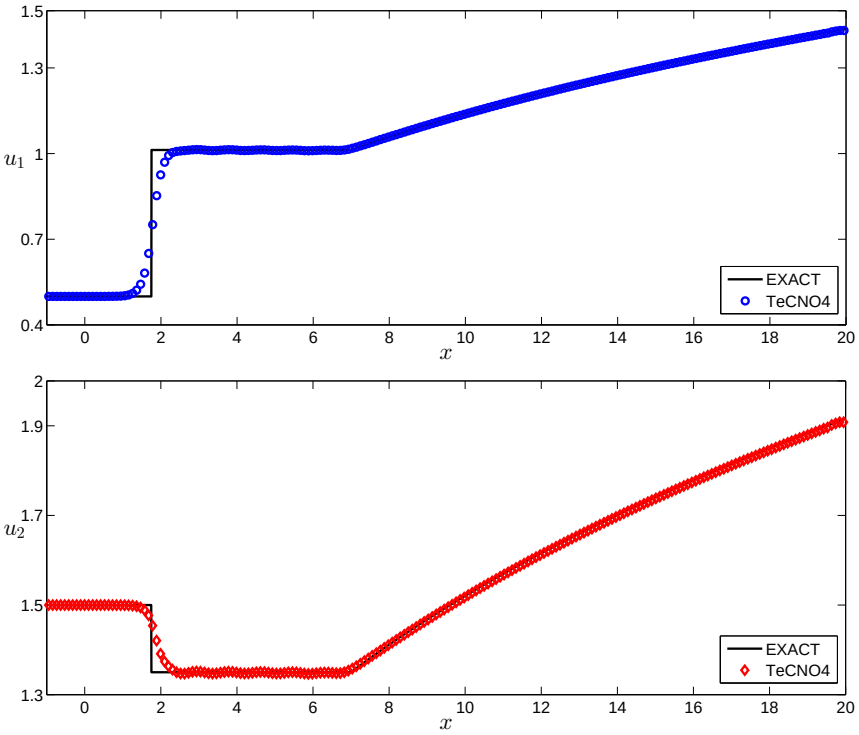

Figure 3: Example 4.2 : Approximate solutions at $t = 0.5$ with $N = 200$ grid points corresponding to the first component (top) and the second component (bottom).

Example 4.3 *Consider the* 2×2 *chromatography system*

$$\boldsymbol{u}_t + \left(\frac{\boldsymbol{u}}{1+r}\right)_x = 0, \quad u_1, u_2 \geq 0, \quad r = u_1 + u_2 \tag{36}$$

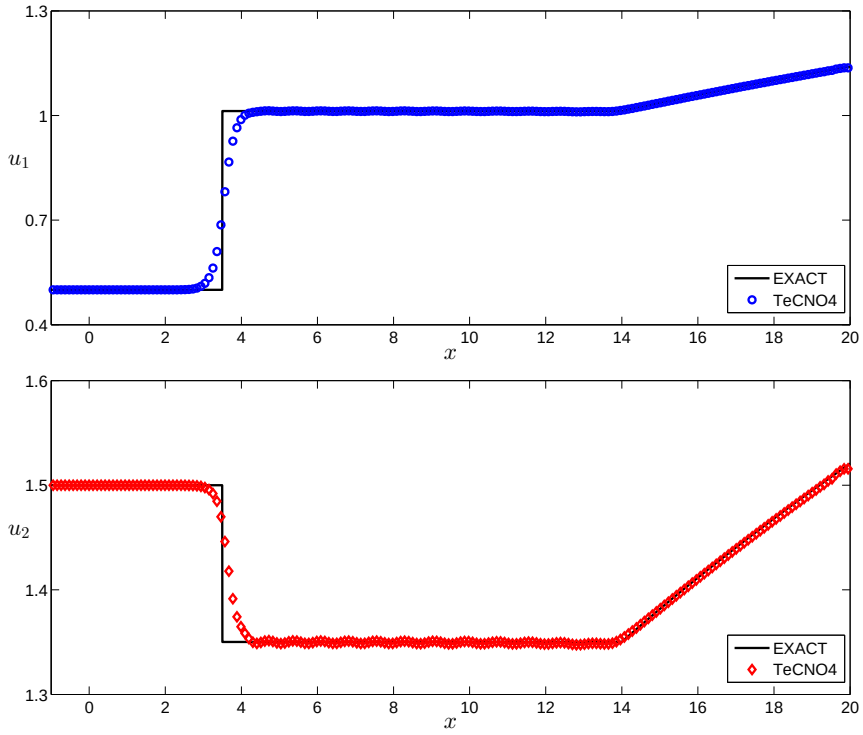

Figure 4: Example 4.2 : Approximate solutions at $t = 1$ with $N = 200$ grid points corresponding to the first component (top) and the second component (bottom).

along with the initial data (31). *The eigenvalues of* (36) *are*

$$\lambda_1(\boldsymbol{u}) = \frac{1}{(1+u_1+u_2)^2} \quad \textit{and} \quad \lambda_2(\boldsymbol{u}) = \frac{1}{1+u_1+u_2},$$

and the corresponding right eigenvectors are $\boldsymbol{r}_1 = \frac{1}{\|\boldsymbol{u}\|}\boldsymbol{u}$ *and* $\boldsymbol{r}_2 = \frac{1}{\sqrt{2}}(1,-1)^{\mathrm{T}}$.
Taking $r_- = \|\boldsymbol{u}_-\|_1 =$ *and* $r_+ = \|\boldsymbol{u}_+\|_1$, *the solutions of the Riemann problem* (36) *have the the following two kinds of combination of elementary waves (see for instance [20])*

Case 1. If $0 < r_- < r_+$, *the Riemann solution is a shock wave* S *followed by a contact discontinuity* J

$$\boldsymbol{u}(x,t) = \begin{cases} \boldsymbol{u}_-, & x < \sigma t, \\ \boldsymbol{u}_*, & \sigma t < x < \lambda_2(\boldsymbol{u}_+)t, \\ \boldsymbol{u}_+, & x > \lambda_2(\boldsymbol{u}_+)t, \end{cases} \tag{37}$$

where $\boldsymbol{u}_*$ *is the intermediate state which is calculated by* $\boldsymbol{u}_* = \frac{\|\boldsymbol{u}_+\|_1}{\|\boldsymbol{u}_-\|_1}\boldsymbol{u}_-$ *and* $\sigma = \frac{1}{(1+r_-)(1+r_+)}$.

Case 2. If $0 < r_+ < r_-$, *the Riemann solution consists of a rarefaction* R *wave and a contact discontinuity* J

$$\boldsymbol{u}(x,t) = \begin{cases} \boldsymbol{u}_-, & x < \lambda_1(\boldsymbol{u}_-)t, \\ \widehat{\boldsymbol{u}}(x/t), & \lambda_1(\boldsymbol{u}_-)t \le x \le \lambda_1(\boldsymbol{u}_*)t, \\ \boldsymbol{u}_*, & \lambda_1(\boldsymbol{u}_*)t < x < \lambda_2(\boldsymbol{u}_+)t, \\ \boldsymbol{u}_+, & x > \lambda_2(\boldsymbol{u}_+)t, \end{cases} \tag{38}$$

where $\boldsymbol{u}_*$ *is the same as above and the rarefaction wave can be given by*

$$\widehat{\boldsymbol{u}}(x/t) = \frac{\sqrt{\frac{t}{x}} - 1}{r_-}\boldsymbol{u}_-.$$

Both configurations $S+J$ *and* $R+J$ *are tested with the initial data* $\boldsymbol{u}_- = (0.8, 1)^{\mathrm{T}}$, $\boldsymbol{u}_+ = (0.2, 1)^{\mathrm{T}}$ *and* $\boldsymbol{u}_- = (0.2, 1)^{\mathrm{T}}$, $\boldsymbol{u}_+ = (0.8, 1)^{\mathrm{T}}$, *respectively. Errors and convergence rates at* $t = 1$ *are presented in Table 3 and numerical solutions are shown in Figure 5.*

	$S+J$				$R+J$			
	u_1		u_2		u_1		u_2	
N	e_1	cr	e_2	cr	e_1	cr	e_2	cr
100	12.35	—	13.44	—	13.62	—	20.39	—
200	7.60	0.700	8.29	0.697	8.50	0.680	12.68	0.685
400	4.64	0.710	4.98	0.733	5.13	0.729	7.50	0.758
800	2.70	0.785	2.85	0.805	2.80	0.875	3.92	0.936
1600	1.45	0.898	1.52	0.901	1.63	0.779	2.17	0.853

Table 3: Example 4.3: approximate L^1-errors ($\times 10^{-3}$) and convergence rates at $t = 1$.

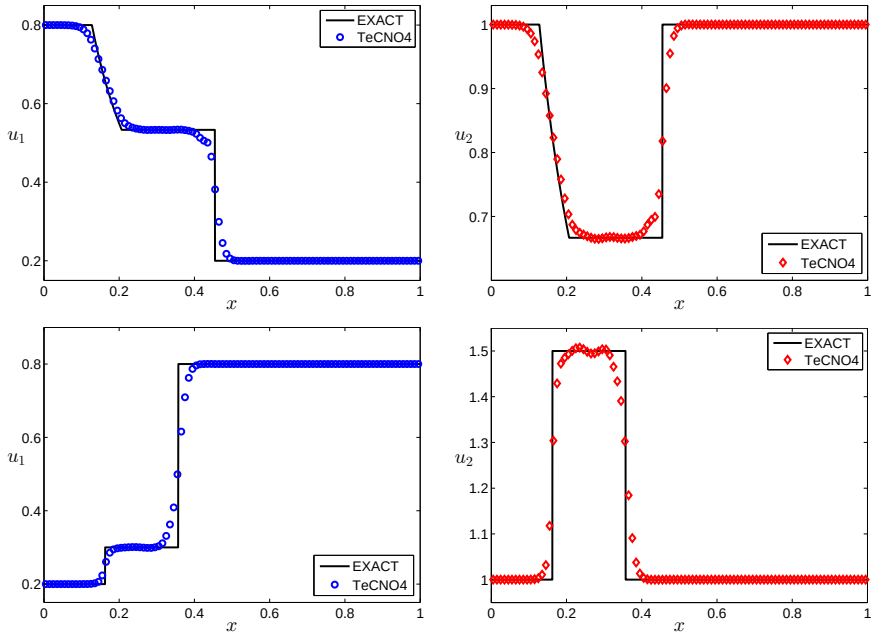

Figure 5: Example 4.3 : Approximate solutions corresponding to the Case 1 (first row) and the Case 2 (second row) at $t = 1$ with $N = 200$ grid points.

5 Conclusions

We have employed high order entropy stables schemes proposed in the literature to obtain numerical solutions for the Keyfitz-Kranzer model. For the symmetric case, the solution is well approximated by the PEC flux strategy which is due to the particular relationship between the eigenvectors and the entropy variables. In comparison to numerical results obtained in other references ([14], [19]), convergence rates presented here have better behavior. It is not possible to obtain an AEC flux in closed algebraic form, even for simple expressions of $\phi(r)$. Then numerical quadratures for approximating the AEC flux was a feasible alternative as it is shown with the good agreement between the exact solutions and numerical solutions.

Acknowledgement

The authors wish to thank the referees for their careful reading of the manuscript and their comments and suggestions.

References

[1] L. Ambrosio, G. Crippa, A. Figalli and L.V. Spinolo, Some new well-posedness results for continuity and transport equations, and applications to the chromatography system, SIAM J. Math. Anal., **41(5)**, 1890-1920 (2009).

[2] S. Benzoni-Gavage and R.M. Colombo, An n-populations model for traffic flow, Eur. J. Appl. Math., **14**, 587-612 (2003).

[3] R.H. Cohen and R.M. Kulsrud, Nonlinear evolution of parallel-propagating hydromagnetic waves, Phys. Fluids, **17(12)**, 2215–2225 (1974).

[4] X. Cheng and Y. Nie, A third-order entropy stable scheme for hyperbolic conservation laws, J. Hyperbolic Differ. Equ., **13(1)**, 129-145 (2016).

[5] X. Cheng, A Fourth Order Entropy Stable Scheme for Hyperbolic Conservation Laws, Entropy, **21(5)**, 508 (2019).

[6] U.S. Fjordholm, S. Mishra and E. Tadmor, Arbitrary high-order essentially non-oscillatory entropy stable schemes for systems of conservation laws, SIAM J. Numer. Anal., **50**, 544-573 (2012).

[7] U.S. Fjordholm, S. Mishra, and E. Tadmor, ENO reconstruction and ENO interpolation are stable, Found. Comput. Math., **13**, 139-159 (2013).

[8] U.S. Fjordholm, S. Mishra, and E. Tadmor, Energy preserving and energy stable schemes for the shallow water equations, In F. Cucker, A. Pinkus, and M. Todd (Eds.), Foundations of Computational Mathematics Proceedings of FoCM held in Hong Kong, 2008. London Math Society Lecture Notes Ser. **363**, 93-139, Cambridge University Press (2009).

[9] U.S. Fjordholm and D. Ray, A sign preserving WENO reconstruction method, J. Sci. Comput., **68**, 42-63 (2016).

[10] S. Gottlieb, C.-W. Shu, and E. Tadmor, Strong stability-preserving high-order time discretization methods, SIAM Review, **43**, 89-112 (2001).

[11] J. C. Hernández, Existence of Weak Entropy Solution for a Symmetric System of Keyfitz-Kranzer Type, Revista Colombiana de Matemáticas, **47(1)**, 13-28 (2013).

[12] F. Ismail and P.L. Roe, Affordable, entropy-consistent Euler flux functions II: Entropy production at shocks, J. Comput. Phys., **228**, 5410-5436 (2009).

[13] B. Keyfitz and H. Kranzer, A System of Non-Strictly Hyperbolic Conservation Laws Arising in Elasticity Theory, Arch. Ration. Mech. Anal., **72**, 219-241 (1980).

[14] U. Koley and N. H. Risebro, Finite difference schemes for the symmetric Keyfitz-Kranzer system, Angew. Math. Phys., **64**, 1057-1085 (2013).

[15] P.G. Lefloch, J.M. Mercier, and C. Rohde, Fully discrete entropy conservative schemes of arbitrary order, SIAM J. Numer. Anal., **40**, 1968-1992 (2002).

[16] M. S. Mock, Systems of conservation laws of mixed type, Journal of Differential equations, **37(1)**, 70-88 (1980).

[17] E. Y. Panov, On the theory of generalized entropy solutions of the Cauchy problem for a class of non-strictly hyperbolic systems of conservation laws, Sb. Math., **191**, 121-150 (2000).

[18] E. Y. Panov, On Infinite-Dimensional Keyfitz-Kranzer Systems of Conservation Laws, Differential Equations, **45**, 274-278 (2009).

[19] N. H. Risebro and F. Weber, A note on front tracking for the Keyfitz-Kranzer system, J. Math. Anal. Appl., 190-199 (2013).

[20] C. Shen, Wave interactions and stability of the Riemann solutions for the chromatography equations, J. Math. Anal. Appl., **365(2)**, 609-618 (2010).

[21] C.-W. Shu, Essentially non-oscillatory and weighted essentially non-oscillatory schemes for hyperbolic conservation laws, In: B. Cockburn, C. Johnson, C.-W. Shu and E. Tadmor, Advanced Numerical Approximation of Nonlinear Hyperbolic Equations (A. Quarteroni, Ed.), Lecture Notes in Mathematics vol. **1697**, Springer-Verlag, Berlin, 325-432 (1998).

[22] D. Ray, Third- Order Entropy Stable Scheme for the Compressible Euler Equations, C. Klingenberg and M. Westdickenberg (eds.) Theory, Numerics and Applications of Hyperbolic Problems II, Springer Proceedings in Mathematics and Statistics **237**, 503-515 (2018).

[23] E. Tadmor, The numerical viscosity of entropy stable schemes for systems of conservation laws, I, Math. Comp., **49**, 91-103 (1987).

[24] E. Tadmor, Entropy stability theory for difference approximations of nonlinear conservation laws and related time-dependent problems, Acta Numerica, **12**, pp. 451–512 (2003).

[25] A. Tveito and R. Winther, Existence, uniqueness and continuous dependence for a system of hyperbolic conservation laws modeling polymer flooding. SIAM J. Math. Anal. **22**, 905–933 (1991)

[26] P. Wang, C. Shen and X. Lin, Construction of global solution for a symmetric system of Keyfitz-Kranzer type with three piecewise constant states, Advances in Difference Equations, (2019), 10.1186/s13662-019-2025-4.